Journal of Colloid and Interface Science 324 (2008) 142–149

Contents lists available at ScienceDirect

Journal of Colloid and Interface Science

www.elsevier.com/locate/jcis

A combined study by XRD, FTIR, TG and HRTEM on the structure of delaminated Fe-intercalated/pillared clay

Peng Yuan [a,*], Faïza Annabi-Bergaya [b], Qi Tao [a,c], Mingde Fan [a,c], Zongwen Liu [d], Jianxi Zhu [a], Hongping He [a], Tianhu Chen [e]

[a] Guangzhou Institute of Geochemistry, Chinese Academy of Sciences, Guangzhou 510640, China
[b] Centre de Recherche sur la Matière Divisée, CNRS-Université d'Orléans, 1b, Rue de La Férollerie, Orléans Cedex 2, France
[c] Graduate School of the Chinese Academy of Science, Beijing 100039, China
[d] The Australian Key Centre for Microscopy and Microanalysis, The University of Sydney, NSW 2006, Australia
[e] School of Natural Resources and Environment, Hefei University of Technology, Hefei 230009, China

ARTICLE INFO

Article history:
Received 7 March 2008
Accepted 30 April 2008
Available online 10 May 2008

Keywords:
Montmorillonite
Pillared clay
Delaminated
Nanoparticles
Iron oxide

ABSTRACT

Fe-PILC samples were synthesized by the reaction between Na^+- and/or Ca^{2+}-montmorillonite (Mt) and base-hydrolyzed solutions of Fe(III) nitrate. Different from the known usual microporous pillared structure, a meso–microporous delaminated structure containing intercalated or pillared fragments was found in the respective resulting Fe-intercalated or -pillared clays. XRD patterns of Na^+-Mt-based Fe-intercalated/pillared clays show one large *d*-spacing above 6.4 nm corresponding to the mesoporous delaminated part, whereas another *d*-spacing of ca. 1.5 nm was indicative of the microporous pillared part. Fe-intercalated/pillared clays based on Ca^{2+}-Mt lead to similar results, but with a *d*-spacing less than 6 nm and a second low intense *d*-spacing less than 1.5 nm. In the delaminated Fe-intercalated clays, NO_3^- anions were retained even after thorough washing process. They play as counterions to neutralize the positive-charged iron aggregates in the delaminated structure, and can be exchanged by heteropolyanions as $[PW_{12}O_{40}]^{3-}$. The delaminated Fe-pillared clays show good thermal stability at 500 °C and exhibit at this temperature dramatically higher specific surface area and porosity than the starting montmorillonites. However, calcination at a higher temperature leads to the formation of nanocrystalline hematite. Air-drying after ethanol extraction (EAD) method has an advantage over air-drying (AD) method in preserving the delaminated structure.

1. Introduction

Pillared interlayered clays (PILC) have attracted continuously increased interest [1] since the first inorganic pillared clay mineral reported in the late 1970s [2]. Classified as a two-dimensional lamellar nanomaterial, PILC is prepared in two steps (i) by exchanging the charge-compensating cations between the swelling clay layers with larger polymeric or oligomeric hydroxy metal cations, leading to intercalated clay minerals, and (ii) by heat treatment of these intercalated clays, the metal hydroxy cations undergo dehydration and dehydroxylation and are transformed to metal oxide (e.g., Al_2O_3 and Fe_2O_3) clusters/nanoparticles, which act as pillars to prop the clay mineral layers apart, and to create a stable microporous pillared structure [1]. The resultant oxide-PILC has shown some promising prospects in the fields of adsorbents and catalysts [3–5].

Much research interests have been directed towards Fe_2O_3-PILC, due to the intrinsic catalytic activities (e.g., as a Fischer–Tropsch catalyst) and the magnetic properties of iron oxide [6–10]. A common route to synthesize Fe_2O_3-PILC is based on the intercalation of iron polycations [4], the base-hydrolyzed product of Fe(III) salts, such as $FeCl_3$ and $Fe(NO_3)_3$. Besides, a synthesis route by intercalation of the trinuclear Fe(III)-acetato complex was also reported in the literatures [11–13].

The interlayer space of Fe_2O_3-PILC synthesized by base-hydrolyzed route appears to be diverse in different reports. Basal spacings $d_{(001)}$ of ca. 2.5 ± 0.4 nm (corresponding to the interlayer space of ca. 1.5 ± 0.4 nm) were reported by several researchers [4,14,15]. In some other reports, however, the basal spacing of Fe_2O_3-PILC is found to be lower than 1.47 nm [7,16,17]. Furthermore, Burch and Warburton and Chen et al., reported the complete disappearance of the regular basal spacing of Fe_2O_3-PILC [18,19], which was proposed to correspond to a delaminated pillared structure. Therefore, some further work are deserved to be done to investigate the structure of Fe_2O_3-PILC, especially the specific formation mechanism of delaminated or pillared structure.

* Corresponding author. Fax: +86 20 85290130.
E-mail address: yuanpeng@gig.ac.cn (P. Yuan).

0021-9797/$ – see front matter
doi:10.1016/j.jcis.2008.04.076

In this work, by using powder X-ray diffraction (PXRD), nitrogen adsorption–desorption isotherms, thermogravimetric (TG) analysis, high-resolution transmission electron microscope (HRTEM) and FTIR spectroscopy, the detailed structural properties were studied, as well as the related anion-exchangeability, of a series of Fe intercalated/pillared montmorillonite samples with delaminated structure. Effects of the starting montmorillonite (Na^+- or Ca^{2+}-Mt) characteristics, drying methods and calcination temperature on the structure of the resultant Fe-PILC samples were also investigated.

2. Materials and methods

2.1. Materials

The calcium-montmorillonite (Ca^{2+}-Mt), supplied by Nanhai Mining Ltd., China, was purified and classified by sedimentation, then the <2 μm fraction was collected for pillaring experiment. The structural formula of the obtained Ca^{2+}-Mt as determined from chemical analysis is:

$$Ca_{0.19}Mg_{0.06}Na_{0.01}(Si_{3.96}Al_{0.04})(Al_{1.44}Fe_{0.09}Mg_{0.47})O_{10}(OH)_2\cdot nH_2O.$$

The cationic exchange capacity (CEC) of the Ca^{2+}-Mt is 66.5 mmol/100 g. The Na^+-montmorillonite (Na^+-Mt) was prepared by ion exchange reaction between Ca^{2+}-Mt and Na_2CO_3, as previously described [20]. Both Ca^{2+}-Mt and Na^+-Mt were used as the starting materials for the pillaring reactions.

The Keggin-type heteropolyanion $[PW_{12}O_{40}]^{3-}$ was prepared by titration of the $H_3PW_{12}O_{40}$ solution (with a pH of ca. 2.0) into a solution of NH_4OH.

2.2. Preparation of iron pillaring solutions and synthesis of PILC

Following a procedure similar to that reported by Rightor et al. [14], Na_2CO_3 powder was slowly added to an aqueous solution of 0.2 M iron(III) nitrate with vigorously stirring (ca. 1100 revs/min). The amount of added base includes six OH/Fe molar ratios in the range of 0.5–2.5. The resulting translucent solution was aged for 24 h at room temperature before addition to the Mt dispersion.

A dispersion of 2 g of starting Mt in 100 ml of deionized water was used. The iron pillaring solution was added dropwise into the vigorously stirred clay dispersion kept in a water bath at 60 °C, with a ratio of 10 mmol Fe per gram of clay. After addition of the pillaring solution, the reaction mixture was stirred for 2 h, and then aged for 20 h at room temperature. The mixture was centrifuged and washed 12 times by successive agitations/centrifugations with deionized water. The obtained wet cakes corresponding to intercalated clay minerals were ready for drying.

2.3. Drying and calcination

Two drying methods, air-drying (shortened hereafter as AD) and air-drying after ethanol extraction (EAD), were used to dry the obtained wet cakes. Under AD condition, wet cakes were dried at 105 °C for 16 h. Under EAD condition, wet cakes were immersed into absolute ethanol, washed and centrifuged with ethanol for 3 times to replace the water by ethanol, then followed by the same steps as for AD condition. A part of the dried intercalated products was ground into powder with mortar for further characterization.

The pillared clay samples were obtained by heating the dried intercalated products for 3 h at different temperatures (300, 400, 500, 600, 700, 800 and 900 °C). The final intercalated or pillared samples were differentiated on the basis of the kind of starting Mt, the OH/Fe molar ratio, the drying method and the calcination temperature. For example, Na^+-Mt-1.0 (AD) denotes the Fe intercalated clay sample, obtained from Na^+-Mt, air-dried, and with a OH/Fe molar ratio = 1.0, while Na^+-Mt-1.0 (AD, 500 °C) represents the pillared counterpart of Na^+-Mt-1.0 (AD) which underwent calcination at 500 °C.

2.4. Exchange reaction

The exchange reaction between the Keggin-type heteropolyanions $[PW_{12}O_{40}]^{3-}$ and the Fe-intercalated sample was carried out by titrating the $[PW_{12}O_{40}]^{3-}$ solution into the Na^+-Mt-1.0 (Fe-intercalated wet cake) with a ratio of 0.4 mmol of heteropolyanions per gram of Na^+-Mt-1.0. The mixture was then stirred for 3 h at 80 °C. The product was separated by centrifugation, washed with deionized water and dried at 105 °C for 16 h.

2.5. Characterization methods

The powder X-ray diffraction (PXRD) patterns were taken on a Rigaku D/max 2550 PC X-ray diffractometer equipped with Ni filter and Cu$K\alpha$ radiation ($\lambda = 0.154$ nm) using a generator voltage of 40 kV and a generator current of 300 mA, and a scan rate of 3° (2θ)/min were applied for the determination.

The chemical composition of the samples was determined using a PE-3100 atomic absorption spectrometer (AAS). The FTIR spectra of the samples were recorded on a Perkin–Elmer 1725X FTIR spectrometer. Specimens for measurement were prepared by mixing 0.9 mg of the sample powder with 70 mg of KBr and pressing the mixture into a pellet. The average over 9 scans was collected for each measurement with a resolution of 2 cm^{-1}.

Conventional TEM images were obtained in a Philips CM120 electron microscope operating at 120 kV. HRTEM characterization and selected-area electron diffraction analysis were preformed on a JEOL 3000F transmission electron microscope with an accelerating voltage of 300 kV. For TEM observation, the clay sample was ultrasonically dispersed in ethanol for 5 min, and then a drop of sample suspension was dropped onto a carbon-coated copper grid, which was left to stand for 10 min and transferred into the microscope.

N_2 adsorption–desorption isotherms were measured at liquid nitrogen temperature with a gas sorption analyzer (Quantachrome, NOVA 1000). Prior to measurement, samples were outgassed at 250 °C at a pressure less than 10^{-3} Torr for at least 3 h. The specific surface area was calculated by the BET equation [21] and the total pore volume was evaluated from nitrogen uptake at a relative pressure of 0.985. The t-plot according to de Boer's method was used to calculate the micropore volume and external surface area [22]. The Barrett–Joyner–Halenda (BJH) method was used to evaluate the average pore diameter (APD) [23]. And the pore size distribution (PSD) curves was fitted by the non-local density functional theory (NLDFT) method [24].

Thermogravimetric (TG) analysis was performed on a Netzsch STA 449C instrument. Approximately 50 mg of finely ground sample was heated in an open corundum crucible. Samples were heated from 40 to 1300 °C at a heating rate of 10 °C/min under highly pure nitrogen atmosphere (20 cm^3/min).

3. Results and discussion

3.1. PXRD and TEM results

Shown in Fig. 1 are the XRD patterns of the starting montmorillonites and the resultant Fe-intercalated samples and Fe-PILC in the low 2θ angle region.

Already, starting Na^+-Mt shows two reflections (Fig. 1a). The first unusual one corresponds to a large d-spacing of 8.2 nm, and the second to a d-spacing of 1.25 nm, attributed to the (001) reflection of Na^+-Mt in temperature and pressure normal conditions. In the cases of Na^+-Mt based Fe-intercalated samples (both AD

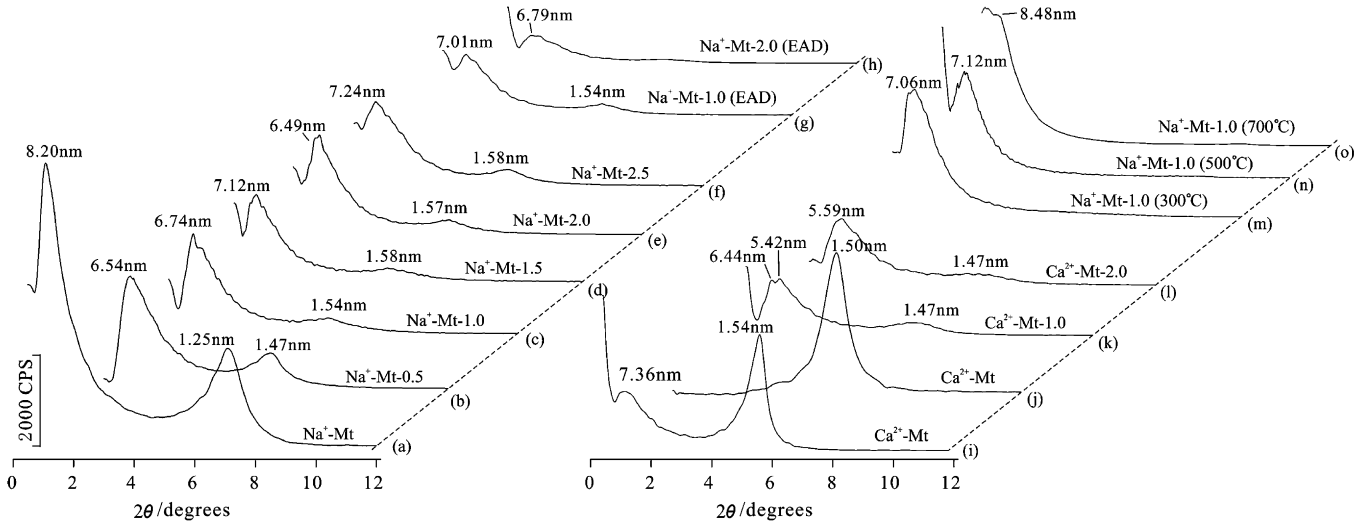

Fig. 1. Powder X-ray diffraction patterns for starting montmorillonites and Fe-intercalated and pillared samples.

and EAD), two *d*-spacings are shown (Fig. 1, b–f for AD and Fig. 1, g and h for EAD). One is in the range 6.49 to 7.24 nm, and another one is in the range 1.47 to 1.58 nm, varying with the OH/Fe molar ratios of pillaring solution. However, the Na^+-Mt based Fe-intercalated samples obtained by EAD exhibit more disordered XRD patterns than those obtained by AD, as indicated by the two related XRD peaks which are weaker and broader.

The pillared samples obtained with Na^+-Mt (AD) and heated at 300 °C, 500 °C and 700 °C, respectively, show only one large reflection increasing with temperature, a peak at 7.06 nm (Fig. 1m), a better defined peak at 7.12 nm (Fig. 1n) and a very broad peak around 8.48 nm (Fig. 1o).

Starting purified Ca^{2+}-Mt also exhibits two *d*-spacings of ca. 7.36 and 1.54 nm (Fig. 1i). The latter one corresponds to the (001) reflection of Ca^{2+}-Mt in temperature and pressure normal conditions. The first XRD peak with large *d*-spacing of Ca^{2+}-Mt has significantly lower intensity than that of Na^+-Mt, nevertheless XRD patterns of Ca^{2+}-Mt based Fe-intercalated samples (AD) (Fig. 1, k and l) are analogous to Na^+-Mt based ones.

It is interesting to note that both starting montmorillonites (Na^+-Mt and Ca^{2+}-Mt) show an unexpected large *d*-spacing (Fig. 1, a and i), respectively. The large *d*-spacing of Ca^{2+}-Mt shows a good duplicability in repeated analyses. However, in repeated measurements the intensity and position of the peak of Na^+-Mt with large *d*-spacing varies a bit with the sample's exposure time in air. Fig. 1a represents the XRD pattern of Na^+-Mt with the largest peak intensity. This result suggests that the structure of Na^+-Mt is more sensitive to ambient humidity than Ca^{2+}-Mt.

The large *d*-spacings shown in Fe-PILC are comparable to that reported by Mandalia et al. [25]. These authors observed for Fe-pillared Mt with OH/Fe ratio of 1.0 and heated at 300 °C, a *d*-spacing of 7.6 nm and a *d*-spacing of 7.2 nm for mixed Al–Fe pillared sample with Fe/(Al + Fe) molar ratio of 0.5 and OH/(Al + Fe) ratio of 1.0. They proposed that these large peaks could be interpreted as large interlayer repeat distances created by mesoporosity between the clay particles [25]. However, in their further investigation on the structure of the above-mentioned Al–Fe pillared samples, they found that the 7.2 nm peak might be a reflection of the distribution of porous structure, rather than being attributed to simple intercalation [26].

In the present work, however, large *d*-spacings are observed in the XRD patterns of starting Na^+-Mt and Ca^{2+}-Mt. This observation confirms the idea that the large *d*-spacing does not correspond to the classic periodic pillared structure of iron species intercalated into the host montmorillonite [26], but corresponds to a disordered porous structure existed even in the starting montmorillonites. Previous studies on some mesoporous disordered solids (e.g., porous silica [27], silica molecular sieves [28,29], and mesoporous biogenetic silica [30]) have shown that disordered mesoporous structure could generate a broad XRD peak in the very low 2θ angle region.

The disordered porous structure in starting montmorillonites might just be the "house of cards" structure resulted from aggregation of clay platelets [31,32]. This structure seems to be formed more easily in Na^+-Mt than in Ca^{2+}-Mt, since the large *d*-spacing of Ca^{2+}-Mt (Fig. 1i) is considerably weaker than that of Na^+-Mt (Fig. 1a). Unlike this purified Ca^{2+}-Mt, a raw Ca^{2+}-Mt sample from Hebei province (China) shows a XRD pattern without the peak with the large *d*-spacing (Fig. 1j), though its derivative Na^+-activated Mt still exhibits a large *d*-spacing at ca. 7.6 nm (not shown here). Considering the raw Ca^{2+}-Mt did not experience any treatment whereas the Ca^{2+}-Mt used here was once purified by water washing and sedimentation, it can be concluded that the water treatment process may have a prominent influence on the porous structure of powdered Mt. Future work focused on this problem is worthwhile to be conducted.

The exhibition of large *d*-spacings of the Fe intercalated and pillared Mt samples (Fig. 1) indicates the formation of a secondary house-of-cards structure, which results from the three-dimensional co-aggregation of clay platelets and the iron hydroxycations or iron oxides nanoparticles. An analogous structure in pillaring treated alumina-clays was called as "delaminated structure" by Pinnavaia et al., who proposed that freeze-drying, rather than air-drying, should be necessary to generate a delaminated structure, since air drying would result in a reorganization of the delaminated aggregates to face-to-face aggregation [31]. Moreover, Occelli et al., have observed the three-dimensional co-aggregation of delaminated structure by HRTEM [33]. However, it is shown by our results that air-drying (AD and/or EAD) can also yield a delaminated structure in Fe-intercalated samples and in Fe-PILC.

The broad peaks centered at 1.5 ± 0.08 nm in the XRD patterns of Fe-intercalated based on Na^+-Mt (Fig. 1, b–f) should be attributed to the (001) reflection. This increase of the $d_{(001)}$ value from 1.25 nm (for Na^+-Mt) to 1.5 ± 0.08 nm (for the resultant Fe-intercalated samples) indicates the intercalation of some small-sized hydrolyzed iron in the interlayer spaces of clay particles. Since the sizes of these iron hydroxycations are not uniform, an inhomogeneous intercalation occurs, consequently different clay particles exhibit different interlayer distances, generating a broad (001) diffraction. This is also evidenced in the Fe-intercalated sam-

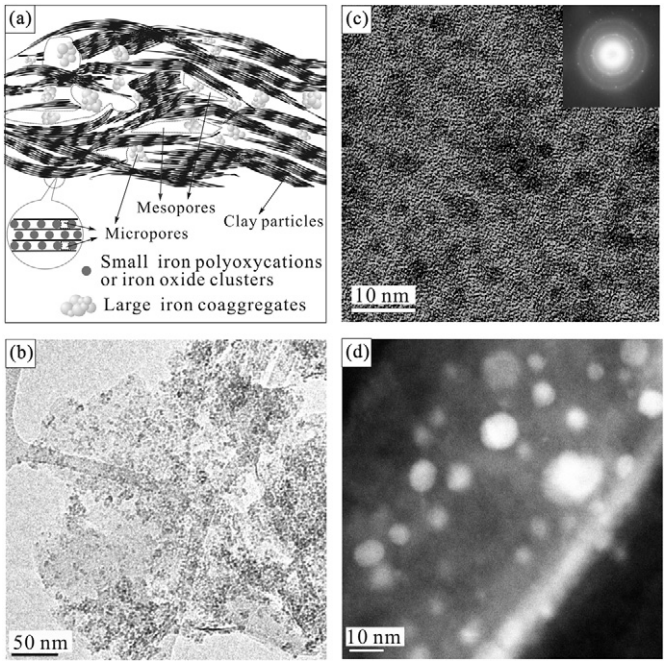

Fig. 2. (a) Schematic representation of a delaminated-pillared structure; (b) TEM micrograph of the sample Na^+-Mt-1.0 (AD); (c) HRTEM bright field image and electron diffraction pattern (the inset); and (d) HRTEM dark field image.

ples based on Ca^{2+}-Mt (Fig. 1, k and l). In the XRD patterns of Fe-PILC (Fig. 1, m–o) this peak becomes too broad to be resolved, suggesting the formation of a much more disordered pillared structure.

Therefore, the resulting Fe-intercalated Mt and Fe-PILC of the present work show a delaminated structure containing intercalated or pillared fragments. They should be referred as delaminated Fe-intercalated clays or Fe-pillared clays. A schematic representation of this delaminated-intercalated/pillared structure is shown in Fig. 2a.

TEM characterization shows that the delaminated Fe-intercalated clays synthesized under different reaction conditions exhibit basically analogous transmission electron micrographs. It should be noticed here that these samples are probably not stable under the TEM conditions, due to the electron beam could generate high temperature and might transform the intercalated particles into pillared particles. Fig. 2b represents a TEM micrograph of the sample Na^+-Mt-1.0 (AD). It can be seen that the iron co-aggregates and the clay platelets are disorderedly stacked together, corresponding to the delaminated part of the proposed delaminated structure. As shown in Figs. 2c and 2d, HRTEM bright field and dark field images of Na^+-Mt-1.0 (AD) reveal that the size of iron oxide co-aggregates/nanoparticles outside the clay interlayer are in the size range 3 to 12 nm, and the mean size of most particles is around 6 nm. The corresponding electron diffraction pattern (Fig. 2c, inset) shows faint rings with plane distances of 0.205, 0.150, 0.120, and 0.103 nm, which are consistent with the iron oxide (332), (622), (811), and (664) plane distances of 0.201, 0.142, 0.116, and 0.100 nm. Therefore, the TEM result supports the proposed delaminated structure.

As mentioned above, the interlayer spaces of Fe_2O_3-PILC synthesized by hydrolysis of iron salts were not consistent in different reports, although the experimental conditions of synthesis were alike. An interesting question arises accordingly, i.e., why some researchers obtained ordered pillared structure whereas those others obtained delaminated ones? Few studies have been conducted to answer this question. Chen et al., proposed that ordered pillared clay resulted from short reaction time (e.g., less than 3 h) at ambient temperature, whereas delaminated pillared clay was formed during long reaction time (e.g., over 12 h) and at higher temperatures (40–50 °C) [19]. However, Canizares et al., did not obtain delaminated structure after 12 h pillaring reaction [15].

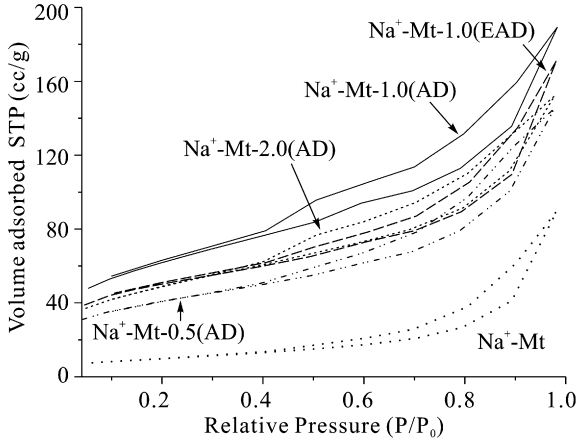

Fig. 3. Nitrogen adsorption–desorption isotherms of Na^+-Mt and Fe-intercalated samples.

In the present work, although a variety of reaction conditions were tried, i.e., changing the reaction time and temperature to synthesize Fe_2O_3-PILC, pillared structure with a characteristic $d_{(001)}$ value beyond 2 nm as reported in the literature [4,14,15] were not obtained, but the delaminated–pillared structure as discussed above was obtained. This result might be reasonable, because hydrolyzed iron cations tend to form discrete polycations spheres with various sizes [34,35]. Consequently, an ordered pillared structure is hard to be yielded. However, more efforts are still worthy to investigate the formation conditions of the pillared structure in Fe-PILC, for instance, to investigate if/how the mineralogical and surface properties of starting Mt could affect the formation of pillared structure.

3.2. BET surface and nitrogen adsorption–desorption isotherms

The nitrogen adsorption–desorption isotherms of Na^+-Mt and Fe-intercalated samples, Na^+-Mt-0.5 (AD), Na^+-Mt-1.0 (AD), Na^+-Mt-2.0 (AD), and Na^+-Mt-1.0 (EAD), are reported in Fig. 3. The other isotherms of intercalated samples appear similar to those shown in Fig. 3. Adsorption isotherm of Na^+-Mt belongs to the type II in the Brunauer, Deming, Deming and Teller (BDDT) classification [36], characteristic of nitrogen adsorption on macroporous adsorbents. The adsorption isotherms of Fe-intercalated samples (AD and/or EAD) belong to type IV, corresponding to mesoporous adsorbents, and present Langmuir adsorption isotherms (type I) in the region of low relative pressure, indicating presence of micropores. Furthermore, the hysteresis loops of these isotherms are assigned to type H3 in the IUPAC classification [22], which is representative of the slit-shaped pores in layered materials. The pore size curves (not shown here) shows a very wide pore size distribution, which well supports our proposed disordered structure which consists of delaminated part with mesoporosity and pillared part with microporosity.

Summarized in Table 1 are the porous structure parameters, including specific surface area (S_{BET}), external surface area ($S_{ext.}$), total pore volume (V_P), microporous volume ($V_{\mu P}$) and average pore diameter (APD). All the samples exhibit a high developed porosity and high surface area as compared with the starting Mt. The largest surface area (215.7 m^2/g) and V_P (0.296 ml/g) are found in Na^+-Mt-1.0 (AD) and Na^+-Mt-2.0 (EAD), respectively. The remarkable mesoporosity of these samples is of particular meaning, since it shows that the hydrolysis of iron salts can provide an alternative

Table 1
Textural properties of the starting montmorillonites, intercalated and pillared samples after heating at 500 °C

Sample	S_{BET} (m^2/g)	$S_{ext.}$ (S_{micro})[a] (m^2/g)	V_P[b] (mL/g)	$V_{\mu P}$ (V_{mP})[c] (ml/g)	APD[d] (nm)
Na^+-Mt	35.1	–	0.138	–	15.76
Na^+-Mt-0.5 (AD)	143.6	113.6 (30.0)	0.224	0.012 (0.212)	6.25
Na^+-Mt-0.8 (AD)	158.2	116.7 (41.5)	0.230	0.018 (0.212)	5.82
Na^+-Mt-1.0 (AD)	215.7	139.8 (75.9)	0.291	0.033 (0.258)	5.39
Na^+-Mt-1.5 (AD)	182.5	120.9 (61.6)	0.245	0.026 (0.219)	5.38
Na^+-Mt-2.0 (AD)	173.4	116.0 (57.4)	0.235	0.024 (0.211)	5.42
Na^+-Mt-2.5 (AD)	177.5	111.1 (66.4)	0.228	0.029 (0.199)	5.13
Na^+-Mt-1.0 (AD, 500 °C)	128.2	102.0 (26.2)	0.196	0.012 (0.184)	6.11
Na^+-Mt-0.5 (EAD)	165.6	139.9 (25.7)	0.271	0.011 (0.260)	6.53
Na^+-Mt-1.0 (EAD)	175.1	126.2 (48.9)	0.264	0.019 (0.235)	6.04
Na^+-Mt-1.5 (EAD)	193.5	156.0 (37.5)	0.251	0.015 (0.236)	5.18
Na^+-Mt-2.0 (EAD)	203.3	155.2 (48.1)	0.296	0.020 (0.276)	5.82
Na^+-Mt-2.5 (EAD)	192.5	137.5 (55.0)	0.279	0.022 (0.257)	5.80
Na^+-Mt-2.0 (EAD, 500 °C)	185.4	150.9 (34.5)	0.287	0.015 (0.272)	6.20
Ca^{2+}-Mt	28.9	–	0.119	–	16.48
Ca^{2+}-Mt-1.0	141.0	90.0 (51.0)	0.183	0.023 (0.160)	5.20
Ca^{2+}-Mt-2.0	174.7	84.9 (89.8)	0.189	0.039 (0.150)	4.34

[a] $S_{ext.}$ = external surface area, evaluated from *t*-plot; surface area of micropore (S_{micro}) is obtained by subtracting $S_{ext.}$ from total surface area (S_{BET}).
[b] V_P = total porous volume.
[c] $V_{\mu P}$ = microporous volume; mesoporous volume (V_{mP}) = $V_P - V_{\mu P}$.
[d] APD = average pore diameter.

Table 2
Main chemical composition of the Fe-pillared samples

Sample	Analytical results (%)			Mol composition[a]
	SiO_2	Al_2O_3	Fe_2O_3	Fe
Na^+-Mt-0.5 (AD)	53.96	10.12	17.83	1.66
Na^+-Mt-0.8 (AD)	52.01	9.26	21.17	2.16
Na^+-Mt-1.0 (AD)	50.04	8.99	24.84	2.61
Na^+-Mt-1.5 (AD)	48.03	8.89	25.36	2.69
Na^+-Mt-2.0 (AD)	47.35	8.62	25.53	2.80
Na^+-Mt-2.5 (AD)	48.27	8.47	30.06	3.35
Na^+-Mt-0.5 (EAD)	55.83	10.09	18.26	1.71
Na^+-Mt-1.0 (EAD)	52.30	8.45	22.50	2.51
Na^+-Mt-1.5 (EAD)	52.12	8.32	24.09	2.73
Na^+-Mt-2.0 (EAD)	49.54	8.28	25.46	2.90
Na^+-Mt-2.5 (EAD)	48.65	7.21	27.49	3.60
Ca^{2+}-Mt-1.0 (AD)	56.39	10.71	15.63	1.38
Ca^{2+}-Mt-2.0 (AD)	51.81	10.71	18.74	1.65

[a] The compositions given in moles for $O_{10}(OH)_2$ anion basis of silicate layer.

way to obtain a mesoporous structure in intercalated and pillared clays, besides the approach of surfactant templating [37–39].

As discussed above, the mesopores in delaminated Fe-intercalated clay and Fe-PILC mainly result from interparticle-spaces generated by three-dimensional co-aggregation of iron polyoxycations or iron oxide nanoparticles. Furthermore, intercalation of small-sized hydrolyzed iron cations or iron oxide clusters generates micropores in the interlayer space of Fe intercalated clay. But the micropores are also originated from the microporous interstice existing among the iron aggregates [40] and/or clay platelets, as schematically represented in Fig. 2a.

From Table 1 it also can be found that Fe intercalated samples for OH/Fe ratio >1, generally have more developed external surface area and porosity under EAD than under AD condition, indicating EAD method has an advantage over AD method in producing high external surface area. This result can be well explained by the fact that ethanol have much lower interfacial tension than water [41], accordingly more pores in delaminated structure under EAD condition can be prevented from collapsing and thus be preserved than those under AD condition.

A relativity can be found between the XRD pattern and the porosity results, e.g., the starting Na^+-Mt with macroporous structure yields a very intense and symmetric XRD peak with large *d*-spacing, nevertheless Na^+-Mt-based Fe intercalated clay minerals with meso–microporous structure yield a weaker and broader peak with a smaller *d*-spacing. In addition, Ca^{2+}-Mt-based Fe intercalated clay samples exhibit much lower surface area and porosity than Na^+-Mt-based ones, as well as weaker XRD peak with large *d*-spacing. These observations suggest that the XRD pattern at low 2θ angles may provide some useful information about the porous structure of clay materials, but so far to know the information specifically is still difficult.

3.3. Chemical analysis, FTIR spectra, and the roles of NO_3^-

Main composition of delaminated Fe-intercalated samples, represented as mass percentage of oxides, are summarized in Table 2. The molar content of iron per $O_{10}(OH)_2$ unit is also given, based on the assumption that the Al_2O_3 content in Mt is unchanged during addition of pillaring solution. The pH values, corresponding to the OH/Fe molar ratios of 0.5, 0.8, 1.0, 1.5, 2.0, and 2.5, of 24 h-aged pillaring solutions are 1.64, 1.66, 1.67, 1.70, 1.72 and 1.90, and those of the final 20 h-aged intercalated mixtures are 1.53, 1.56, 1.58, 1.64, 1.70 and 1.95, respectively. These pH values are consistent with those reported by Rightor et al. [14]. Increase of OH/Fe molar ratio in the initial pillaring solution leads to a remarkable increase of the iron content of the Fe-pillared products. And at same OH/Fe molar ratio, the content of introduced iron species follows this order of delaminated intercalated samples: Na^+-Mt-based (EAD) > Na^+-Mt-based (AD) > Ca^{2+}-Mt-based (AD).

Fig. 4 shows the FTIR spectra (400–2000 cm^{-1}) of starting Mt and the intercalated and pillared clay minerals. The wavenumber and assignment of each vibration mode observed are listed in Table 3. The assignments are based on previous reports on Mt and polyoxometalates samples [42,43]. It should be noticed that due to the vibration modes of the iron oxide/hydroxide species (e.g., 470 cm^{-1} of the Fe–O vibration, 1000 cm^{-1} of the Fe–O–H vibration, etc.) overlapped with those of Mt (Fig. 4), the vibration mode of iron species is not well resolved in the IR spectra.

A vibration mode at ca. 1384 cm^{-1}, attributed to the NO_3^- stretching mode, is shown in the FTIR spectra of Na^+-Mt-based Fe-intercalated Mt (AD). It is of particular interest that the intensity of peak of NO_3^- strongly increases with the OH/Fe molar ratio from 0.5 to 2.5 (Fig. 4, b–g). An analogous dependency of the intensity

Table 3
Positions and assignments of observed IR vibration bands

Position (cm^{-1})	Assignments	Position (cm^{-1})	Assignments
1630	OH bending of water	916	Al–Al–OH deformation
1435	CO_3 stretching of calcite	799 and 883	W–O–W stretching of $[PW_{12}O_{40}]^{3-}$
1384	NO_3 stretching	842	Al–Mg–OH deformation
1092	Si–O stretching of cristobalite	796	Si–O stretching of cristobalite
1081	P–O stretching of $[PW_{12}O_{40}]^{3-}$	624	Coupled Al–O and Si–O, out of plane
1034	Si–O stretching	519	Al–O–Si deformation
982	W=O stretching of $[PW_{12}O_{40}]^{3-}$	470	Si–O–Si deformation/Fe–O stretching

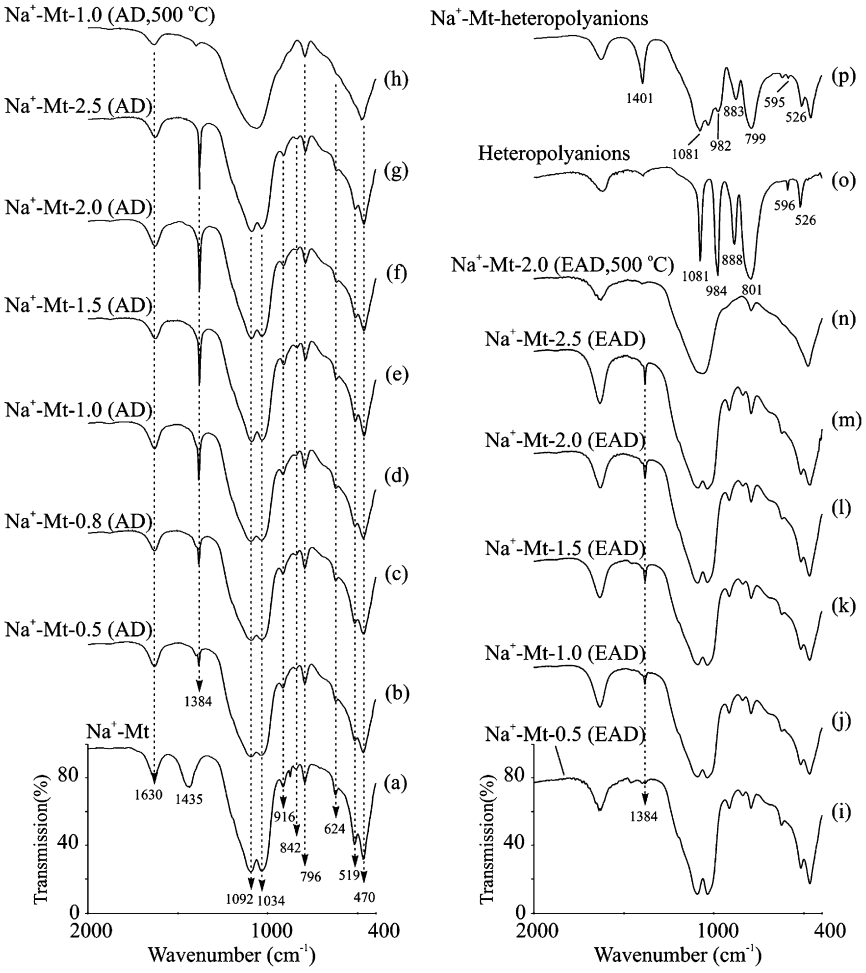

Fig. 4. FTIR spectra for starting Mt and Fe-intercalated and pillared samples.

of NO_3^- band on the OH/Fe ratio is observed in the spectra (Fig. 4, i–m) of Na^+-Mt-based Fe-intercalated Mt (EAD) but the change in intensity is less spectacular. In the pillared samples heated at 500 °C (Fig. 1, h and n) this peak is very weak.

In a classical pillared structure of PILC, anions such as Cl^- and NO_3^- would be washed away by repeated agitation and centrifugation. However, a large amount of NO_3^- is retained in the dried intercalated samples of the present work, despite a thorough washing process applied in present work. Accordingly, the occurrence of NO_3^- reflects that there exist some redundant positive-charged iron aggregates outside the interlayer space of Mt, and the NO_3^- anions act as counterions to neutralize the redundant positive charge present in the interparticles. This can be used to explain why the intensity of NO_3^- band increases with the content of introduced iron species, as shown in Table 2 and Fig. 4. Consequently, the FTIR results match well with the proposed structure of delaminated structure.

The presence of NO_3^- in these samples is of academic importance, since NO_3^- could be utilized as an exchangeable site for other anions, and the content of NO_3^- could be controlled to some extent by adjusting the OH/Fe ratio. As shown in Fig. 4, o and p, in the spectrum of the product of reaction between Na^+-Mt-1.0 (AD) and $[PW_{12}O_{40}]^{3-}$, the band of NO_3^- disappears whereas the vibration mode of $[PW_{12}O_{40}]^{3-}$ appears, indicating that NO_3^- in Na^+-Mt-1.0 was exchanged by $[PW_{12}O_{40}]^{3-}$. This exchangeability of the NO_3^- by heteropolyanions, e.g., $[PW_{12}O_{40}]^{3-}$ as mentioned above, might be of significance in catalytic application. Further work is underway to investigate the acidity of this novel heteropolyanions-exchanged Mt and to explore its reactivity as a heterogeneous catalyst. In contrast with the Fe-intercalated sample derived from cationic Mt, previously only anionic clays such as layered double hydroxides (LDH) are known to have the property of anion exchangeability and have been used in the catalytic field [44,45].

As summarized from Tables 1 and 2, and Fig. 4, the OH/Fe molar ratio of the initial pillaring solution shows a prominent influence on the meso–microporous structure and the chemical composition of Fe-intercalated samples. At low OH/Fe mole ratio (<1.0), iron cations are hydrolyzed to primary products with low molecular weight and small size, some of which could be intercalated into the clay interlayer. However, at high OH/Fe mole ratios, more hydrated iron cations tend to aggregate [40,46–48], and the resultant large-sized iron aggregates remain outside the interlayer space and overlap the clay particles to form the delaminated structure. As a result, more NO_3^- anions are retained to neutralize the positive charge in the interparticle space.

At a same OH/Fe molar ratio, Na^+-Mt-based delaminated Fe-intercalated Mt exhibits an advantage over Ca^{2+}-Mt-based one in resulting in more developed porosity and higher content of iron species, indicating that Na^+-Mt is more suitable than Ca^{2+}-Mt for being used as the starting materials for preparation of these delaminated materials.

Furthermore, at same OH/Fe molar ratio, the lower content of NO_3^- seen in Fig. 4, for samples dried by EAD method than those by AD method, seems in contradiction with the chemical analysis result which shows that the content of iron species in samples dried by EAD is higher than that by AD, which should lead to a

higher content of NO_3^-. This mismatch indicates that NO_3^- is more easily washed away from the wet cake by ethanol than by water.

3.4. Effect of thermal treatment temperatures on the delaminated Fe-PILC

As shown in Fig. 1, m–o, the (001) reflections disappear in the XRD patterns of samples thermally treated above 300 °C, indicating the loss of the periodic pillared structure, thus the formation of a more disordered structure. On the other hand, the XRD peak of large *d*-spacing shows fluctuation in intensity and position, indicating some changes of the porosity occurring in the delaminated porous structure. Compared to Na^+-Mt-1.0 (AD), Na^+-Mt-1.0 (AD, 500 °C) shows an obvious decrease in surface area and microporous volume, but its mesoporosity is mostly preserved (Table 1). This result reflects that in the pillared–delaminated structure, the delaminated part has stronger thermal stability than the interlayer pillared part. This proposal is well supported by the fact that the delaminated structure is better preserved in the intercalated structure obtained by EAD than those obtained by AD. For example, Na^+-Mt-2.0 (EAD, 500 °C) exhibits only a small decrease in surface area and mesoporosity compared to Na^+-Mt-2.0 (EAD), as shown in Table 1.

Another dramatic change occurring in calcined delaminated Fe-PILC is the evaporation and/or decomposition of most NO_3^- and OH^- in clay structure, as revealed by FTIR spectra (Fig. 4, h and n). The loss of NO_3^- and OH^- might result in the formation of Lewis acid sites, based on a similar mechanism found in dehydroxylated PILC [49]. This can explain the unexpected high acidity of a previously reported Fe-pillared clay [17], which exhibited a basal spacing of ca. 1.47 nm but containing much more acid sites after calcination than conventional Al-PILC.

The TG and DTG curves of Na^+-Mt-2.0 (AD) are similar to those of Na^+-Mt-2.0 (EAD) (Figs. 5a and 5b). The obvious weight-loss at 61 °C corresponds to desorption of the physically adsorbed water, however, the FTIR result shows the existence of O–H vibration of water even at 500 °C (Fig. 4, h and n). This contrast indicates that the rehydration of the samples occurred under FTIR analysis, and the desorption temperature of water was decreased under *in situ* heating condition of thermogravimetric analysis.

The weak weight loss at ca. 210 °C should be attributed to the dehydroxylation of Fe polyoxycations and/or decomposition of NO_3^-. The weight-loss at 583–653 °C denotes the dehydroxylation of clay layer. However, the accurate assignment for the weight-loss at ca. 755 (AD) and 948 °C (EAD) of Na^+-Mt-2.0 seems to be difficult. They might reflect some phase transformation occurring at those temperatures accompanying by loss of weight. Consistent with the analysis results on surface area and porosity, the TG and DTG results also show that delaminated Fe-intercalated samples obtained by EAD is more thermally stable than those obtained by AD.

Fig. 5c shows that nanocrystalline hematite phase was formed in Na^+-Mt-1.0 (AD) when the calcination temperature is increased to 600 °C. However, it was reported that pure polymeric iron(III) corresponding to akaganeite is easily transformed to hematite (seen by Mossbauer) at a much lower calcination temperature at 300 °C [50,51]. Therefore, the delaminated structure shows advantages in improving the thermal stability of iron aggregates, probably because the clay particles not only separated the iron aggregates, but also actually behaved as barriers to prevent the aggregates from further agglomeration to form hematite nanocrystalline phase under calcination.

Further increase of temperature results in increase of the size of nanoparticles of crystalline hematite. The mean diameter, *D*, of the hematite nanocrystallites in thermally treated delaminated clay mineral (Fe-PILC) can be estimated by the Scherrer equation

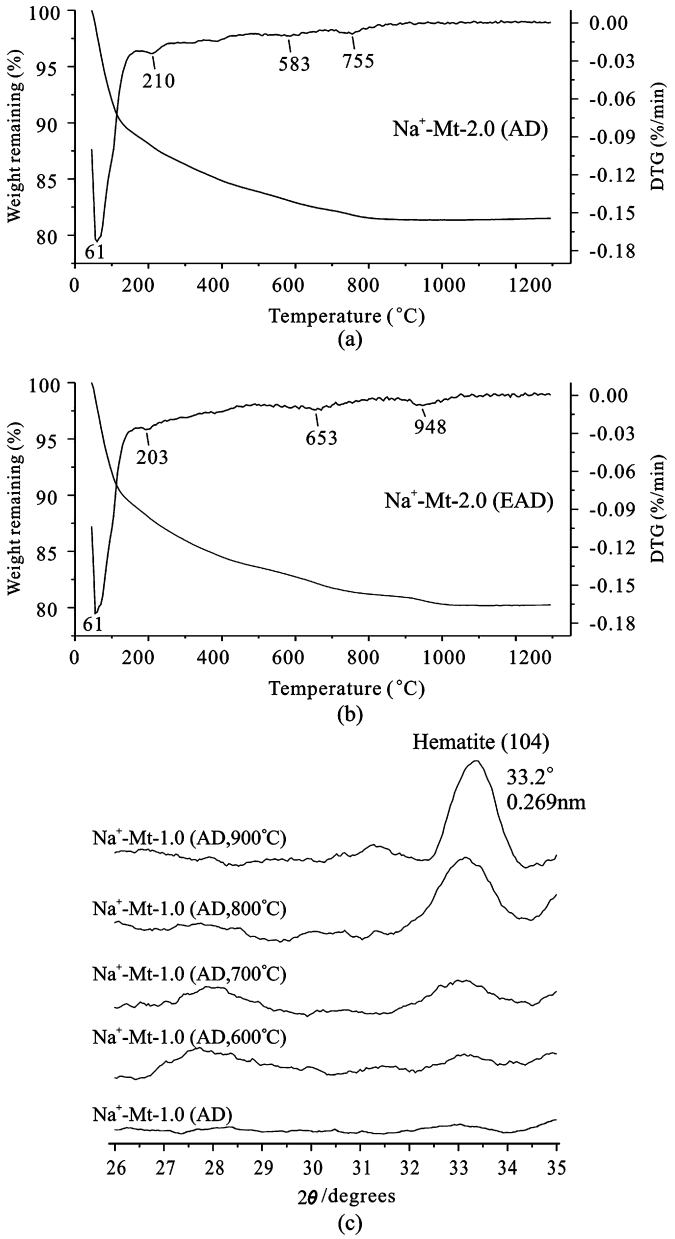

Fig. 5. TG and DTG curves of (a) Na^+-Mt-2.0 (AD) and (b) Na^+-Mt-2.0 (EAD); (c) the XRD patterns of Na^+-Mt-1.0 (AD) calcined at different temperatures.

($D = k\lambda/\beta\cos\theta$), where k is the shape factor with the value of 0.9, β is the line broadening which is the breadth of the diffraction line at its half intensity maximum, λ is the radiation wavelength applied and θ is the Bragg angle. Here the Bragg angle θ (i.e., 33.2/2°) corresponding to the reflection of hematite (104) crystallographic plane is used for the calculation (Fig. 5c). The calculated D values of the hematite crystallites in Na^+-Mt-1.0 (AD) samples calcined at 600, 700, 800 and 900 °C are 15.9, 17.3, 20.3 and 23.2 nm, respectively. Considering nano-size effect is very useful to improve the reaction efficiency as generally reported [52], the formation of hematite nanoparticles above 600 °C in delaminated Fe-PILC and the adjustable size of the nanoparticles are useful for related applications.

4. Summary

Iron intercalated then pillared clays synthesized by base-hydrolyzed route shows a meso–microporous structure composed

of delaminated pillared particles. Resulting from the overlapping clay particles by iron aggregates outside the clay interlayer, the mesoporous delaminated structure corresponds to the large *d*-spacing in XRD pattern. Due to the existence of the positive-charged iron aggregates outside the clay interlayer, NO_3^- anions are retained as counterions in the delaminated structure, and can be exchanged by functional anions such as heteropolyanions $[PW_{12}O_{40}]^{3-}$. The content of NO_3^- is positively dependent on the content of iron aggregates, which can be adjusted by the OH/Fe molar ratio of the initial pillaring solution.

Air-drying after ethanol extraction (EAD) method shows advantages over air-drying (AD) method in preserving the delaminated structure in delaminated Fe-intercalated and pillared clays. And Na^+-Mt is more suitable than Ca^{2+}-Mt for being used as the starting clay for preparation of delaminated Fe-intercalated clays.

The delaminated porous structure shows good thermal stability at 500 °C. On the other hand, the temperature of phase transformation from iron aggregates to nanocrystalline hematite is dramatically increased due to the clay particles which act as heat-insulated barriers.

These fundamental results derived from this study are of meaning in understanding the detailed characteristics of the delaminated structure of Fe_2O_3-PILC, as well as in applying delaminated Fe_2O_3-PILCs as novel heterogeneous catalysts and adsorbents.

Acknowledgments

Financial supports from Natural Science Foundation of China (Grant No. 40672036), Knowledge Innovation Program of the Chinese Academy of Sciences (Grant No. Kzcx2-yw-112), National High Technology Research and Development Program of China (Grant No. 2006AA03Z337) and Natural Science Foundation of Guangdong Province, China (Grant No. 5006267) are gratefully acknowledged. The authors would like to thank Dr. D. Yang, Prof. F.Y. Wang, Prof. D.Q. Wu, Prof. Y.M. Zhang, Dr. W.S. Xiao, and Dr. Q. Zhou for their assistance in XRD analysis, BET measurement, IR analysis, and in improving the manuscript.

References

[1] F. Bergaya, A. Aouad, T. Mandalia, in: F. Bergaya, B.K.G. Theng, G. Lagaly (Eds.) Handbook of Clay Science Developments of Clay Science, vol. 1, Elsevier Science, Amsterdam, 2006, p. 393.
[2] G.W. Brindley, R.E. Sempels, Clay Miner. 12 (1977) 229.
[3] R.T. Yang, L.S. Cheng, in: J.T. Pinnavaia, M.F. Thorpe (Eds.), Access in Nanoporous Materials, Kluwer Academic Publishers, New York, 1995, p. 73.
[4] J.T. Kloprogge, J. Porous Mater. 5 (1998) 5.
[5] Z. Ding, J.T. Kloprogge, R.L. Frost, G.Q. Lu, H.Y. Zhu, J. Porous Mater. 8 (2001) 273.
[6] S. Yamanaka, T. Doi, M. Hattori, Mater. Res. Bull. 19 (1984) 161.
[7] D.H. Doff, N.H.J. Gangas, J.E.M. Allan, J.M.D. Coey, Clay Miner. 23 (1988) 367.
[8] F. Bergaya, J. Barrault, in: I.V. Mitchell (Eds.), Pillared Layered Structures. Current trends and applications, Elsevier Science, Amsterdam, 1990, p. 167.
[9] F. Bergaya, N. Hassoun, L. Gatineau, J. Barrault, in: G. Poncelet, P.A. Jacobs, P. Grange, B. Delmon (Eds.), Preparation of Catalysts V, Elsevier Science, Amsterdam, 1991, p. 329.
[10] J. Barrault, L. Gatineau, N. Hassoun, F. Bergaya, Energy Fuels 6 (1992) 760.
[11] M.A. Martin-Luengo, H. Martins-Carvalho, J. Ladriere, P. Grange, Clay Miner. 24 (1989) 495.
[12] N. Maes, E.F. Vansant, Microporous Mater. 4 (1995) 43.
[13] L. Huerta, A. Meyer, E. Choren, Microporous Mesoporous Mater. 57 (2003) 219.
[14] E.G. Rightor, M.S. Tzou, T.J. Pinnavaia, J. Catal. 130 (1991) 29.
[15] P. Canizares, J.L. Valverde, M.R.S. Kou, Microporous Mesoporous Mater. 29 (1999) 267.
[16] W.Y. Lee, R.H. Raythatha, B.J. Tatarchuk, J. Catal. 115 (1989) 159.
[17] H.M. Mody, P.M. Oza, V.P. Pandya, J. Indian Chem. Soc. 70 (1993) 11.
[18] R. Burch, C.I. Warburton, Appl. Catal. 33 (1987) 395.
[19] J.P. Chen, M.C. Hausladen, R.T. Yang, J. Catal. 151 (1995) 135.
[20] H.P. He, R.L. Frost, F. Deng, J.X. Zhu, X.Y. Wen, P. Yuan, Clays Clay Miner. 52 (2004) 350.
[21] S.J. Gregg, K.S.W. Sing, Adsorption, Surface Area and Porosity, second ed., Academic Press, London, 1982.
[22] J.H. de Boer, B.G. Linsen, Th. van der Plas, G.J. Zondervan, J. Catal. 4 (1965) 649.
[23] E.P. Barrett, L.G. Joyner, P.P. Halenda, J. Am. Chem. Soc. 73 (1951) 373.
[24] S. Lowell, J.E. Shields, M.A. Thomas, M. Thommes, Characterization of Porous Solids and Powders: Surface Area, Pore Size and Density, Kluwer Academic, Boston, 2004.
[25] T. Mandalia, M. Crespin, D. Messad, F. Bergaya, Chem. Commun. 19 (1998) 2111.
[26] C. Clinard, T. Mandalia, D. Tchoubar, F. Bergaya, Clays Clay Miner. 51 (2003) 421.
[27] P. Levitz, D. Tchoubar, J. Phys. I 2 (1992) 771.
[28] S.A. Bagshaw, E. Prouzet, T.J. Pinnavaia, Science 269 (1995) 1242.
[29] S.A. Bagshaw, T.J. Pinnavaia, Angew. Chem. Int. Ed. Engl. 35 (1996) 1102.
[30] E.F. Christabel, H. Yannick, V. Loic, L. Benedicte, Chem. Phys. Lett. 398 (2004) 414.
[31] T.J. Pinnavaia, M.S. Tzou, S.D. Landau, R.H. Raythatha, J. Mol. Catal. 27 (1984) 195.
[32] G. Lagaly, S. Ziesmer, Adv. Colloid Interface Sci. 100–102 (2003) 105.
[33] M.L. Occelli, J.V. Senders, J. Lynch, J. Catal. 107 (1987) 557.
[34] T.G. Spiro, S.E. Allerton, J. Renner, A. Terzis, R. Bils, J. Am. Chem. Soc. 88 (1966) 2721.
[35] J.M. Oades, Clays Clay Miner. 32 (1984) 49.
[36] S. Brunauer, L.S. Deming, W.S. Deming, W.J. Teller, J. Am. Chem. Soc. 62 (1940) 1723.
[37] C.T. Kresge, M.E. Leonowicz, W.J. Roth, J.C. Vartuli, J.S. Beck, Nature 359 (1992) 710.
[38] S. Inagaki, Y. Fukushima, K. Kuroda, Chem. Commun. 3 (1993) 680.
[39] H.Y. Zhu, Z. Ding, J.C. Barry, J. Phys. Chem. B 106 (2002) 11420.
[40] J.Y. Bottero, A. Manceau, F. Villieras, D. Tchoubar, Langmuir 10 (1994) 316.
[41] Z. Ding, H.Y. Zhu, G.Q. Lu, P.F. Greenfield, J. Colloid Interface Sci. 209 (1999) 193.
[42] J. Madejova, P. Komadel, Clays Clay Miner. 49 (2001) 410.
[43] C. Rocchiccioli-Deltcheff, M. Fournier, R. Franck, R. Thouvenot, Inorg. Chem. 22 (1983) 207.
[44] T. Kwon, T.J. Pinnavaia, Chem. Mater. 1 (1989) 381.
[45] T. Polubesova, T. Undabeytia, S. Nir, L. Chertkova, H. Van Damme, F. Bergaya, J. Environ. Qual. 29 (2000) 948.
[46] P.J. Murphy, A.M. Posner, J.P. Quirk, J. Colloid Interface Sci. 56 (1976) 270.
[47] C.M. Flynn, Chem. Rev. 84 (1984) 31.
[48] D. Tchoubar, J.Y. Bottero, P. Quienne, M. Amaud, Langmuir 7 (1991) 398.
[49] T.J. Bandosz, K. Cheng, J. Colloid Interface Sci. 191 (1997) 456.
[50] B. Tian, H. Tang, Environ. Chem. 9 (1990) 70 (in Chinese).
[51] A. Aouad, A.S. Anastacio, F. Bergaya, J.W. Stucki, Clays Clay Miner. (2008), in press.
[52] H. Van Damme, F. Bergaya, L. Gatineau, J. Chim. Phys. 84 (1987) 1075.